3092 *Biochemistry* **2010,** *49,* 3092–3100
DOI: 10.1021/bi901726c

BIOCHEMISTRY
including biophysical chemistry & molecular biology
Article

Differential Effects of Divalent Manganese and Magnesium on the Kinase Activity of Leucine-Rich Repeat Kinase 2 (LRRK2)

Brian Lovitt,[‡] Erica C. VanderPorten,[‡] Zejuan Sheng,[§] Haitao Zhu,[§] Jake Drummond,[‡] and Yichin Liu*[,‡]

[‡]*Biochemical Pharmacology and Early Leads and* [§]*Department of Neuroscience, Genentech, Inc., One DNA Way, South San Francisco, California 90480*

Received October 7, 2009; Revised Manuscript Received March 1, 2010

ABSTRACT: Various mutations in leucine-rich repeat kinase 2 (LRRK2) have been linked to susceptibility for both familial and idiopathic late-onset Parkinson's disease (PD). In this study, we have demonstrated that phosphorylation of MBP and LRRKtide by the LRRK2 G2019S mutant was activated by Mn^{2+} *in vitro*. This enhanced G2019S kinase activity was due to the combination of an increase in kinase and a decrease in ATPase activity by Mn^{2+}. Compared to 10 mM Mg^{2+}, 1 mM Mn^{2+} reduced ATP K_m for G2019S from 103 to 1.8 μM and only modestly reduced k_{cat} (2.5-fold); as a result, the Mn^{2+} increased its k_{cat}/K_m by 22-fold. This change in ATP K_m was due in large part to an increase in nucleotide affinity. While Mn^{2+} also increased ATP affinity and had similar effects on k_{cat}/K_m for LRRK2 WT and R1441C enzymes, it reduced their k_{cat} values significantly by 13−17-fold. Consequently, the difference in the kinase activity between G2019S and other LRRK2 variants was enhanced from about 2-fold in Mg^{2+} to 10-fold in Mn^{2+} at saturating ATP concentrations relative to its K_m. Furthermore, while Mg^{2+} yielded optimal V_{max} values at Mg^{2+} concentration greater than 5 mM, the optimal Mn^{2+} concentration for activating LRRK2 catalysis was in the micromolar range with increasing Mn^{2+} above 1 mM causing a decrease in enzyme activity. Finally, despite the large but expected differences in IC_{50} tested at 100 μM ATP, the apparent K_i values of a small set of LRRK2 ATP-competitive inhibitors were within 5-fold between Mg^{2+}- and Mn^{2+}-mediated reactions except AMP-CPP, an ATP analogue.

Leucine-rich repeat kinase 2 (LRRK2)[1] is a 2527 amino acid long protein comprised of a number of protein−protein interaction domains including N-terminal ankyrin repeats (ANK), a leucine-rich repeat region (LRR), and a C-terminal WD40 domain (Figure 1A). This large protein also hosts a Ras of complex (Roc) GTPase domain and a kinase domain with the two enzyme domains flanking a linker region called C-terminus of Roc (COR) (Figure 1A) (*1*). While multiple interacting partners and protein chaperons of LRRK2 have been characterized (e.g., Hsp70, Hsp90, microtubules) (*2*−*5*), the physiologically relevant substrates of LRRK2 have not yet been identified or confirmed. Current studies involving biochemical characterization of the enzyme activity have utilized autophosphorylation (*6*), phosphorylation of myelin basic protein (MBP) (*7*), or phosphorylation of the peptide substrate derived from ezrine/moesin/radixin (*8*). Recent human genetics findings have linked multiple mutations at different regions of LRRK2 to the susceptibility of both familial and sporadic Parkinson's disease (PD) (*1*, *9*). Among the mutations identified, G2019S found in the kinase domain is the most common mutation, and this mutant has been shown to have higher kinase activity *in vitro* (*7*). Other mutations such as I2020T in the kinase domain and R1441C and Y1699C in the Roc domain have not been consistently shown to affect kinase activity *in vitro* (*8*, *10*, *11*). It has been suggested that various cofactors, including GTP and manganese, are required for LRRK2 optimal kinase activity (*12*, *13*). The modulation of kinase activity by the GTPase domain is thought to parallel the interaction between GTP-bound Ras and its kinase effectors; thus LRRK2's PD-linked mutations located in the Roc domain have been proposed to augment kinase activity indirectly by enhancing GTP binding, inhibiting GTP hydrolysis, or changing protein conformation (*14*−*16*).

Previously, Luzon-Toro and colleagues have suggested that manganese is required for LRRK2 kinase activity (*13*) despite the commonly accepted view that magnesium, which is more abundant in cells (*17*), is the physiologically relevant divalent ion used by kinases (*18*) and the fact that the majority of published LRRK2 reactions were carried out in the presence of divalent magnesium. The most common G2019S mutation is located in the highly conserved Mg^{2+}-binding D(F/Y)G domain where the mutated residue is N-terminal to the activation loop (Figure 1A) (*7*, *8*). It has been hypothesized that a conserved small residue like glycine at this position would allow for maximal conformational flexibility of the activation loop that is required for modulating kinase activity (*19*). Consequently, mutations of the glycine residue could either disrupt the ordering of the magnesium binding domain and the activation loops or might lock the loop in the active conformation that typically is induced upon phosphorylation within the activation loop (*7*, *19*, *20*). Even though LRRK2 does contain, upstream to the catalytic D1994, an arginine residue that is conserved among kinases that are regulated through activation segment phosphorylation (*21*), neither phosphorylations nor changes in the conformation of the activation loop have been demonstrated to be the regulatory mechanism of LRRK2 kinase activity. Understanding how cofactors such as GTP or divalent

*To whom correspondence should be addressed. Telephone: (650) 467-4648. Fax: (650) 467-6045. E-mail: liu.yichin@gene.com.

[1]Abbreviations: LRRK2, leucine-rich repeat kinase 2; PD, Parkinson's disease; MBP, myelin basic protein; LDH, lactic acid dehydrogenase; PK, pyruvate kinase; 5-FAM, fluorescein-5-carboxamide.

 Published on Web 03/05/2010

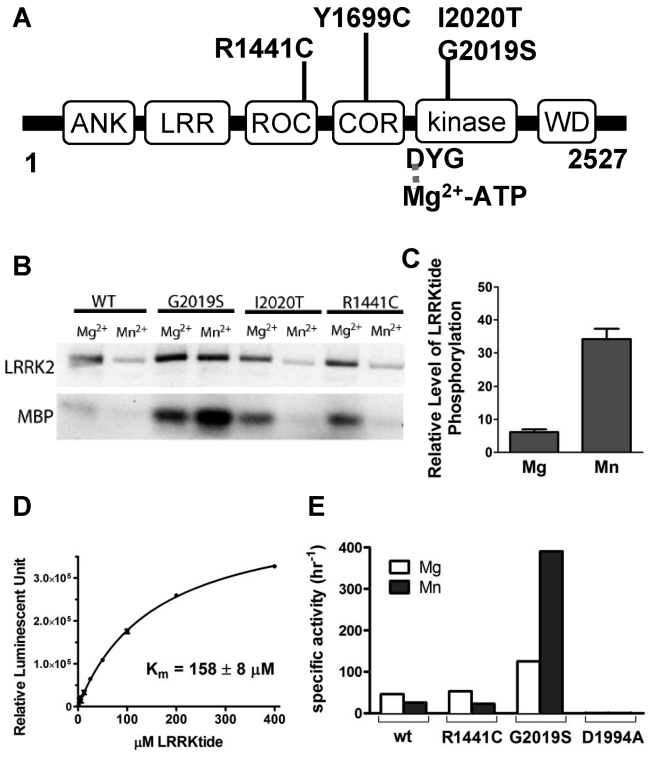

FIGURE 1: Phosphorylation activity of LRRK2. (A) Schematic representation of LRRK2's domain structure and the most commonly known PD-linked mutations. (B) Autophosphorylation and phosphorylation of MBP using [γ-^{33}P]ATP were compared among WT, G2019S, I2020T, and R1441C variants in reaction buffer containing either 10 mM $MgCl_2$ or 1 mM $MnCl_2$. Phosphorylation of MBP by G2019S was significantly enhanced by Mn^{2+}. (C) Using a capillary electrophoresis assay that directly monitored the phosphopeptide product formation, the phosphorylation of FAM-LRRKtide by G2019S was also increased in the presence of Mn^{2+} as compared to Mg^{2+}. (D) LRRKtide K_m measured in Mn^{2+} reaction buffer using G2019S and a luciferase-based assay was similar to the reported values using Mg^{2+} (*8*, *10*). (E) Kinase activity on LRRKtide was compared among LRRK2 variants in Transcreener ADP^2 assay using 10 μM ATP. G2019S showed increased catalytic turnover of ATP in the presence of Mn^{2+} compared to Mg^{2+} by ~3-fold, while WT and R1441C showed a decrease. The kinase inactive mutant D1994A did not yield observable activity in either condition.

ions regulate LRRK2 enzyme activities can potentially provide clues in explaining how the enzymatic function of LRRK2 is associated with the onset and progression of PD. In this study, we demonstrated that different divalent ions (magnesium vs manganese) have significant impact on the catalytic activity of LRRK2. Compared to Mg^{2+}, Mn^{2+} increased k_{cat}/K_m of LRRK2 kinase activity by lowering the ATP K_m by about 100-fold. The increase in the nucleotide binding to LRRK2, however, was accompanied by a significant reduction (13−17-fold) in k_{cat} for all proteins except the G2019S mutant. As a result, the differential kinase activity of the G2019S mutant relative to other LRRK2 variants was enhanced in the Mn^{2+}-mediated reaction compared to Mg^{2+} at saturating ATP concentrations relative to their respective ATP K_m.

MATERIALS AND METHODS

Reagents, Proteins, and Peptides. All variants (WT, G2019S, R1441C, D1994A) of GST-tagged LRRK2 containing amino acids 970−2527 (lacking only the ANK domain) were purchased from Invitrogen (Madison, WI). LRRKtide (RLGRDKYKTLRQIRQ) and FAM-LRRKtide (5-FAM-GAGRLGRDKYKTLRQIRQ) were synthesized by American Peptide Co. (Sunnyvale, CA). Transcreener ADP^2 detection reagents were purchased from Bellbrook Laboratories (Madison, WI). EasyLite kinase luminescence reagents were purchased from Perkin-Elmer (Waltham, MA) and Kinase-Glo Max luminescent kinase assay reagent was purchased from Promega (Madison, WI).

Radiometric LRRK2 Kinase Assay. Autophosphorylation and myelin basic protein (MBP) phosphorylation by LRRK2 were assessed using 120 nM LRRK2 enzymes in the presence or absence of 0.2 μg of MBP in kinase reaction buffer (50 mM HEPES, pH 7.5, and 5 mM DTT) containing either 1 mM $MnCl_2$ or 10 mM $MgCl_2$. The kinase reactions were initiated by addition of 50 μM ATP spiked with 20 μCi of [γ-^{33}P]ATP (Perkin-Elmer) and were incubated at 30 °C for 30 min in a final reaction volume of 10 μL. Reactions were terminated by the addition of lithium dodecyl sulfate sample buffer (Invitrogen) followed by heating at 70 °C for 10 min. Denatured proteins were separated on SDS−PAGE and analyzed by autoradiography.

Transcreener ADP^2 and EasyLite Luciferase Assays for Kinase Reaction. Unless stated otherwise, kinase reactions (4 μL) containing 1 nM LRRK2 G2019S, 100 μM LRRKtide substrate, and 10 μM ATP in kinase reaction buffer (50 mM HEPES, pH 8.0, 0.003% Triton X-100, 5 mM DTT, and either 1 mM $MnCl_2$ or 10 mM $MgCl_2$) were incubated at ambient temperature for 75 min in low-volume 384- or 1536-well black plates. To quench kinase reactions and detect ADP production, 3 μL of Transcreener ADP^2 detection mixture containing 20 mM EDTA, 15 μg/mL anti-ADP antibody, and 8 nM ADP AlexaFluor633 tracer were added into the kinase reactions. The ADP in the assay was detected by measuring the change in the fluorescence polarization of the ADP AlexaFluor633 tracer upon binding to anti-ADP in the presence of enzyme-catalyzed ADP production. The final mixture was allowed to equilibrate at ambient temperature for 30 min. Fluorescence polarization was detected with either an EnVision multilabel plate reader (Perkin-Elmer) using the optimized Cy5 FP dual emission label from Perkin-Elmer (excitation filter, nonpolarized Cy5 620/40; emission filters, Cy5 FP S-pol 688/45 and Cy5 FP P-pol 688/45; optical module, Cy5 FP D658/fp688 dual mirror) or Wallac ViewLux (Perkin-Elmer) plate reader using Alexa 594 dichroic mirror in combination with 618/8 excitation filter and 671/7.8 emission filter. Luciferase-coupled luminescence ATP detection was performed by adding 3 μL of EasyLite reagent (Perkin-Elmer) to the 4 μL kinase reaction and allowing reaction mixtures to equilibrate at ambient temperature for 10 min. Luminescence was measured with either an EnVision multilabel plate reader or Wallac ViewLux.

LRRKtide and ATP K_m Determinations. LRRKtide K_m was determined using 200 μM ATP and various concentrations of LRRKtide in the Mn^{2+}-containing reaction buffer described above. The catalytic ATP turnover was measured using Kinase-Glo Max luminescent kinase assay (Promega). ATP K_m was determined in kinase reactions using the same Mn^{2+} and Mg^{2+} reaction buffers described above with 500 μM LRRKtide substrate. In Mn^{2+} reaction buffer, WT, G2019S, and R1441C LRRK2 enzymes were tested at 10, 1, and 8 nM, respectively, and at 7, 2, and 4 nM, respectively, in Mg^{2+} reaction buffer. A 2-fold serial dilution of ATP from 400 to 0 μM was added to the enzyme to initiate reactions and then quenched in 10 min intervals from 0 to 60 min. Anti-ADP antibody concentration used in the detection reagent was unique to each ATP concentration and

was 2× of the EC_{85} values calculated using the linear correlation equation (eq 1) provided by Bellbrook Laboratories:

$$EC_{85}\ \text{ADP antibody}\ (\mu g/mL) = 0.51 \times \mu M\ \text{ATP} + 0.4 \quad (1)$$

Standard curves were generated for each ATP concentration in both Mn^{2+} and Mg^{2+} reaction buffers, and the quantity of micromolar ADP produced was determined for each reaction at each time point. Initial velocities of ADP production were calculated by measuring the slope of the linear region of each reaction as a function of time. The initial velocities up to 10% ATP conversion obtained were then plotted against ATP concentrations and fitted to a Michaelis−Menten plot using GraphPad Prism 5 (La Jolla, CA) to obtain k_{cat}, V_{max}, and K_m values.

Continuous spectrophotometric measurement of ATP conversion to ADP by LRRK2 phosphorylation of LRRKtide was also measured in a pyruvate kinase−lactate dehydrogenase coupled assay. LRRK2 (88 nM WT, 100 nM G2019S, or 230 nM R1441C) was prepared in reaction buffer containing 50 mM HEPES, pH 8.0, 0.003% Triton X-100, 5 mM DTT, 1 mM phosphoenolpyruvate (Sigma), 1 mM NADH (Sigma), 18.6 units/mL pyruvate kinase (Sigma), 22.7 units/mL lactate dehydrogenase (Sigma), and 500 μM LRRKtide with either 1 mM $MnCl_2$ or 10 mM $MgCl_2$. The reaction was initiated by addition of a 2-fold serial dilution of ATP (200 to 0 μM in Mn^{2+} reaction buffer and 4000 to 0 μM in Mg^{2+} reaction buffer). The reaction progress was monitored by NADH absorbance at 340 nm for 6 h using a Spectramax plate reader (Molecular Devices). The change in absorbance at 340 nm was plotted against time, and the initial rates were calculated. Initial velocities were then plotted against ATP concentrations and fitted to a Michaelis−Menten plot to determine V_{max} and K_m values. k_{cat} was calculated as micromoles per second of product produced per micromole of enzyme.

IC_{50} and K_i Determinations. A panel of Sigma LOPAC compounds were screened in single point followed by dose response against G2019S LRRK2 in both Mn^{2+}- and Mg^{2+}-containing reaction buffers as described above for Transcreener ADP^2 assays. IC_{50} values were converted to K_i using the Cheng−Prusoff equation (*22*) where the K_m values of ATP were 1.8 μM in Mn^{2+} buffer and 103 μM in Mg^{2+} buffer.

Active Site Competitive Florescence Polarization Binding Assay. Compound binding affinities to G2019S and WT LRRK2 were assessed using a florescence polarization-based competitive binding assay. The EC_{85} values of the binding curves were determined to be 15 and 30 nM using 2 nM kinase tracer 236 (Invitrogen) for G2019S and WT variants, respectively, in an enzyme titration experiment. LRRK2 G2019S (15 nM) and WT (30 nM) was preincubated with a 2-fold serial dilution of compounds (3000 to 0 μM) in reaction buffer (50 mM HEPES, pH 7.2, 0.003% Triton X-100, 5 mM DTT, and 1 mM $MnCl_2$ or 10 mM $MgCl_2$) for 30 min at ambient temperature. Two nanomolar kinase tracer 236 (Invitrogen) was added to a final reaction volume of 9 μL, and kinase tracer 236 binding to the kinase active site was allowed to equilibrate for 30 min. Fluorescence polarization was measured on the EnVision multilabel plate reader (Perkin-Elmer) using the optimized Cy5 FP dual emission label.

Microfluidic Capillary Electrophoresis Assay. LRRK2 reactions were carried out in a final volume of 40 μL per well in a 384-well microplate. A standard enzymatic reaction, initiated by the addition of 20 μL of 2× ATP to 20 μL of 2× enzyme, contained 10 nM G2019S, 1 μM FAM-LRRKtide, 12.5 μM ATP, 25 mM Tris, pH 8.0, 1 mM $MnCl_2$ or 5 mM $MgCl_2$, 0.01% Triton X-100, 2 mM DTT, 5 mM β-glycerophosphate, 5 mM NaF, 100 μM Na_3VO_4, and 1× protease inhibitor cocktail (Calbiochem). After incubation for 120 min at ambient temperature, the product and substrate in each reaction were separated using a 12-sipper microfluidic chip (Caliper Life Sciences, Hopkinton, MA) run on a Caliper LC3000 (Caliper Life Sciences, Hopkinton, MA). The separation of product and substrate was optimized by choosing voltages and pressure using Caliper's optimizer software (Hopkinton, MA). The separation buffer contained 100 mM HEPES, pH 7.2, 0.015% Brij-35, 0.1% coating reagent 3, 10 mM EDTA, and 5% DMSO. The separation conditions used a downstream voltage of −500 V, an upstream voltage of −2350 V, and a screening pressure of −1.4 psi. The product and substrate fluorescence was excited at 488 nm and detected at 530 nm. Substrate conversion was calculated from the electrophoregram using HTS Well Analyzer software (Caliper Life Sciences, Hopkinton, MA).

RESULTS

Divalent Manganese Enhances Phosphorylation of MBP and LRRKtide by LRRK2 G2019S. The observation of differential effects of divalent ions on the catalytic activity of kinases has been reported previously (*23*, *24*), with Mg^{2+} as a generally preferred activator for serine/threonine kinases and Mn^{2+} often preferred by tyrosine kinases (*24*). In this study LRRK2, a serine/threonine kinase, was shown to have higher autophosphorylation and MBP substrate phosphorylation activities in the presence of Mg^{2+}, with the exception of the G2019S variant (Figure 1B). While Mn^{2+} yielded a comparable level of G2019S autophosphorylation compared to Mg^{2+}, MBP phosphorylation by G2019S was significantly enhanced by the presence of Mn^{2+}. This result suggests that there may be differences in substrate recognition and the rate of ATP turnover between G2019S kinase and autophosphorylation mediated by the two divalent ions. This type of differential effects between kinase and autophosphorylation activities by various divalent metal ions has also been observed previously in p21-activated protein kinase, γ-PAK (*23*). Consistent with the MBP phosphorylation data, a 6-fold enhancement in G2019S kinase activity by Mn^{2+} was also observed with a peptide substrate derived from ezrin/moesin/radixin (LRRKtide) (*8*) using capillary electrophoresis assays (Figure 1C). The LRRKtide K_m with Mn^{2+} was shown to be comparable (K_m = 158 ± 8 μM) to those reported for reactions carried out in the presence of Mg^{2+} (*8*, *10*) (Figure 1D). This result is different from the activation of C-terminal Src kinase (CSK) where Mn^{2+} was shown to lower the K_m of the poly(Glu, Tyr) peptide substrate when compared to the K_m obtained with Mg^{2+} (*25*). A comparison of catalytic ATP turnover in the presence of 100 μM LRRKtide substrate among LRRK2 WT, G2019S, and R1441C also confirmed the unique activation of kinase activity of the G2019S variant by Mn^{2+} (Figure 1E). Neither Mg^{2+} nor Mn^{2+} produced observable activity in the kinase inactive mutant D1994A, suggesting that the differential enzyme activities were intrinsic to LRRK2 proteins and not due to kinase contaminants from protein purification. In the presence of Mn^{2+}, LRRK2 G2019S kinase activity was about 10-fold greater than WT and R1441C variants while only a 2−3-fold increase was observed with Mg^{2+} buffer (Figure 1E). This modest level of difference in G2019S kinase activity compared to WT observed in Mg^{2+}-mediated reactions is consistent with previously reported values (*19*).

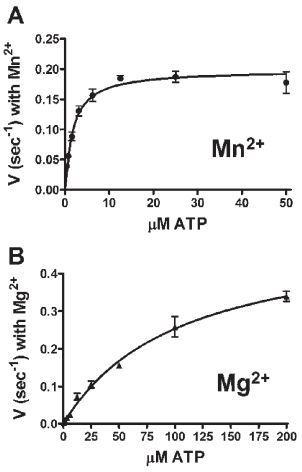

C

LRRK2		K_m (μM)	k_{cat} (sec^{-1})	k_{cat}/K_m (sec^{-1} μM^{-1})
WT	Transcreener Assay			
	Mg	49.5 ± 5.5	0.450 ± 0.021	0.009
	Mn	0.2 ± 0.1	0.028 ± 0.002	0.140
	LDH-coupled Assay			
	Mg	61.3 ± 10.6	0.184 ± 0.007	0.003
G2019S	Transcreener Assay			
	Mg	103 ± 14	0.517 ± 0.037	0.005
	Mn	1.8 ± 0.2	0.200 ± 0.006	0.111
	LDH-coupled Assay			
	Mg	364 ± 45	0.155 ± 0.007	0.0004
R1441C	Transcreener Assay			
	Mg	34.0 ± 6.2	0.367 ± 0.024	0.011
	Mn	0.4 ± 0.1	0.027 ± 0.001	0.068
	LDH-coupled Assay			
	Mg	42.7 ± 5.9	0.162 ± 0.005	0.004

FIGURE 2: Michaelis−Menten plots of ATP titration against G2019S in either (A) Mn^{2+} or (B) Mg^{2+} reaction buffer using the Transcreener ADP^2 detection assay. (C) Comparison of ATP K_m and k_{cat} values with the two divalent ions for WT, G2019S, and R1441C.

Divalent Ions Modulate K_m and k_{cat} of ATP Catalysis. To understand how divalent metal ions regulate catalysis of ATP by LRRK2 variants, steady-state kinetic profiles were characterized in Transcreener ADP^2 assay for WT, G2019S, and R1441C variants. First, the apparent K_m values of ATP measured in the presence of 500 μM LRRKtide (excess to the peptide K_m) and 10 mM Mg^{2+} were found to be 49.9, 103, and 34.0 μM for WT, G2019S, and R1441C, respectively. These values are comparable to those previously reported (*10*, *26*). However, in contrast to previous reports that G2019S has an approximately 4−5-fold higher k_{cat} in a radiometric assay (*10*), our current studies showed that the G2019S k_{cat} value (0.517 ± 0.037 s^{-1}) increased only modestly compared to the WT and R1441C values (0.450 ± 0.021 s^{-1} and 0.367 ± 0.024 s^{-1}, respectively) (Figure 2C). The ATP K_m and k_{cat} determination using a LDH/PK-coupled assay also confirmed the rank order of K_m values among the LRRK2 variants in the presence of Mg^{2+} and the lack of a significant enhancement of k_{cat} for G2019S (Figure 2C). In the presence of 1 mM Mn^{2+}, the Transcreener ADP^2 assay showed an increase in k_{cat}/K_m for all LRRK2 variants (Figure 2C). This change in the catalytic efficiency is largely due to ∼100-fold lower ATP K_m compared to the values obtained with Mg^{2+}, suggesting that different divalent ions have significant impacts on ATP binding affinity at the LRRK2 kinase active site. While changing divalent ions from Mg^{2+} to Mn^{2+} resulted in a large reduction in ATP K_m for all three LRRK2 variants tested, it significantly decreased the maximum catalytic rate of WT and R1441C by 13−17-fold while affecting the G2019S k_{cat} more modestly by only 2.5-fold. Because of the differential impacts on the k_{cat} that Mn^{2+} had among LRRK2 variants, the enhancement of G2019S kinase activity on LRRKtide relative to WT and R1441C is more pronounced in the Mn^{2+}-mediated reaction than the activation observed with Mg^{2+} at the saturating ATP concentration relative to their respective ATP K_m values. These results can also explain the selective increase in LRRKtide phosphorylation by G2019S using 10 or 12.5 μM ATP in the presence of Mn^{2+} (Figure 1C,E). At 10 μM concentration, ATP is in excess to the ATP K_m for all LRRK2 enzymes in reactions containing Mn^{2+}; thus the enhanced phosphorylation activity is predominantly reflected by k_{cat} rather K_m. In contrast, 10 μM ATP in reactions containing Mg^{2+} is below ATP K_m for all LRRK2 variants tested; thus the kinase activity is affected by both K_m and k_{cat} values. Because of the large reduction in k_{cat} for WT and R1441C by Mn^{2+}, even with ATP concentrations at 5.0- and 3.4-fold lower than their respective ATP K_m values obtained with Mg^{2+}, the phosphorylation activity in the presence of Mn^{2+} is still expected to be lower compared to Mg^{2+}. G2019S at 10 μM ATP, in contrast, showed an expected 4−6-fold higher LRRK2 phosphorylation activity in Mn^{2+}-mediated reactions (5.5-fold > ATP K_m) compared to Mg^{2+} (10-fold < ATP K_m). Taken together, these data also emphasize the importance of considering ATP concentration relative to the ATP K_m determined under specific reaction conditions with peptide or protein substrates when interpreting the different degrees of kinase activation as reported *in vitro* by the G2019S mutation (*19*).

Effect of Mg^{2+} and Mn^{2+} Concentrations on ATP K_m and V_{max}. To characterize the concentration dependency of divalent ions on LRRK2 catalytic activity, ATP K_m and V_{max} values for G2019S were determined in the titration experiments of each metal ion. Increasing amounts of Mg^{2+} (1.25, 2.5, 5, and 10 mM) resulted in an increase in V_{max} by greater than 2-fold without affecting apparent ATP K_m values (91 ± 18 μM, 107 ± 26 μM, 119 ± 25 μM, and 103 ± 21 μM, respectively) (Figure 3A). A plot of the apparent V_{max} versus [Mg^{2+}] showed that the maximum reaction velocity reached a plateau at 5 mM Mg^{2+} (Figure 3B). Mg^{2+} tested below 1 mM yielded lower apparent ATP K_m values for G2019S (43 ± 13 μM with 0.625 mM Mg^{2+}) suggesting that the formation of the ATP−metal complex reached saturation at approximately 1 mM Mg^{2+}. This result is similar to that demonstrated for CSK where ATP−Mg complex formation reached saturation with 1 mM Mg^{2+} but additional Mg^{2+} could further activate the enzyme's catalytic rate (*27*). In contrast to the Mg^{2+} experimental results, increasing concentration of Mn^{2+} from 0.625, 2.5, 5, to 10 mM resulted in an overall 4.5-fold decrease in the apparent ATP K_m values (2.7 ± 0.4 μM, 1.4 ± 0.5 μM, 1.0 ± 0.2 μM, and 0.6 ± 0.2 μM, respectively) (Figure 3C). Furthermore, increasing levels of Mn^{2+} were shown to reduce V_{max} values with the optimal Mn^{2+} concentration below the lowest tested concentration of 625 μM (Figure 3C,D). These opposite effects on both the K_m and V_{max} values between varying concentrations of Mg^{2+} and Mn^{2+} suggest (1) an inhibitory mechanism specific to high concentration of Mn^{2+} and/or (2) potentially two divergent metal−ATP−enzyme interactions at the phosphotransfer transition state. These data also suggest that the observed 2.5-fold difference in k_{cat} between 10 mM Mg^{2+} and 1 mM Mn^{2+} for G2019S might be further minimized by using Mn^{2+} at micromolar

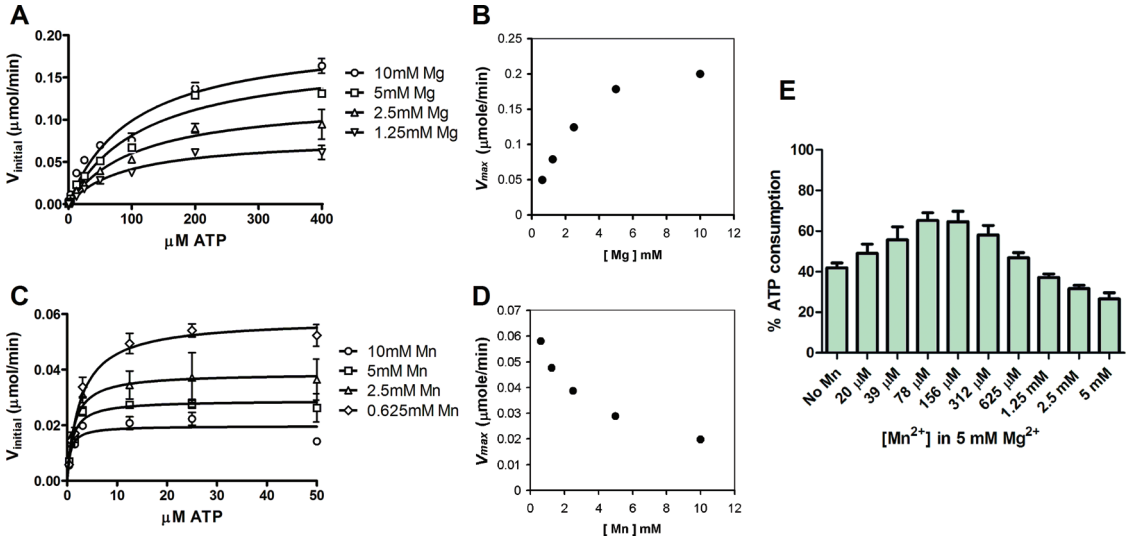

FIGURE 3: Effects of divalent ion concentration on G2019S catalytic activity measured in the Transcreener ADP^2 assay. (A, B) The V_{max} of the enzyme reaction was enhanced with increasing concentrations of Mg^{2+} reaching saturation at 5 mM. (C, D) Mn^{2+} showed the opposite effect with LRRK2 V_{max} increasing as Mn^{2+} concentration was reduced below 1 mM. For Mg^{2+}, ATP K_m values were not affected by the concentration of the divalent ion while increasing concentration of Mn^{2+} resulted in an overall slight decrease in the apparent ATP K_m values. (E) A titration of Mn^{2+} in the presence 5 mM Mg^{2+}, 10 μM ATP, and 50 μM LRRKtide was performed in a luciferase-based ATP detection assay. Increasing concentration of Mn^{2+} enhanced the ATP turnover with maximum activity observed at Mn^{2+} concentration ranging between 78 and 156 μM.

concentration, which would also be closer to its known cellular concentration (*28*).

Micromolar Mn^{2+} Activates G2019S Activity in the Presence of Millimolar Mg^{2+}. To assess potential impacts of the large cellular molar ratio difference between the two divalent ions on the ability of Mn^{2+} to modulate LRRKtide-dependent G2019S kinase activity, a titration of Mn^{2+} was performed in the presence of 5 mM Mg^{2+} where the catalytic rate for G2019S reached its plateau. Increasing concentration of the Mn^{2+} enhanced the LRRKtide-dependent ATP turnover, and the activation reached a maximum at Mn^{2+} concentration ranging between 78 and 156 μM (Figure 3E). This optimal concentration range is consistent with conditions found for optimal V_{max} values observed in the Mn^{2+} titration experiment. This result thus demonstrates that even in the presence of the vast excess amount of Mg^{2+} that mirrors the cellular environment Mn^{2+} is still capable of exerting its activating effect on G2019S kinase activity.

LRRK2 Enzymes Have ATPase Activity That Can Be Minimized by Mn^{2+}. In the absence of peptide substrate LRRKtide, recombinant LRRK2 enzymes displayed significant ATPase activity with the commonly used 10 mM Mg^{2+} buffer (Figure 4A). Comparing LRRK2 variants (WT, G2019S, R1441C, and D1994A), the relative enzyme-dependent ATP hydrolysis rates were parallel to the relative kinase activities (G2019S > WT = R1441C > D1994A) (Figure 4A), suggesting that contaminating proteins such as HSP90 (known to be associated with LRRK2) (*4*) were unlikely to be the source of the observed ATPase activity. These data also support the hypothesis that the phosphorylation and ATP hydrolysis activities of LRRK2 are processed through the same enzymatic active site. Using the Transcreener ADP^2 assay, the rate of ATP turnover was compared between Mg^{2+}- and Mn^{2+}-containing buffers in the absence of the LRRKtide substrate. Similar to the reaction conditions carried out using 100 μM LRRKtide, WT and R1441C enzymes had decreased rates of ADP production with 10 μM ATP substrate and no peptide when the divalent ion in the assay was switched from Mg^{2+} to Mn^{2+}. The kinase

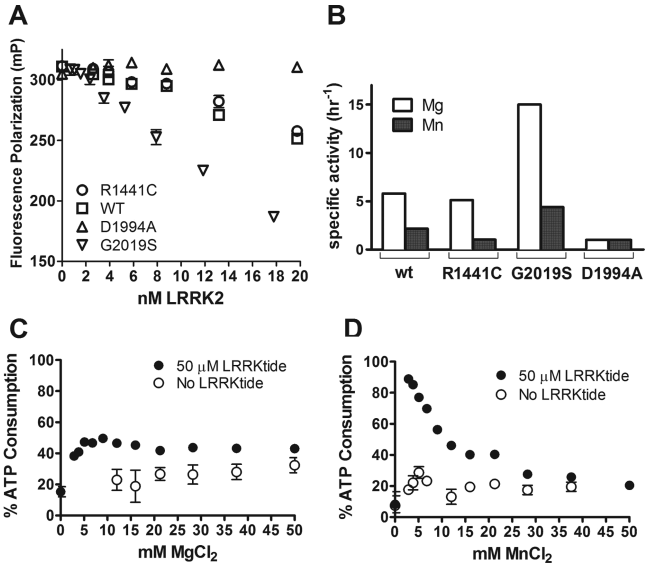

FIGURE 4: ATPase activity of LRRK2 enzymes. (A) Using the Transcreener ADP^2 assay in which a decrease in fluorescence polarization of detection tracer (*Y*-axis) corresponds to an increase in ADP production, LRRK2 showed enzyme concentration-dependent ATP turnover in the absence of LRRKtide substrate. Among the LRRK2 variants tested, G2019S showed the greatest ATPase activity. WT and R1441C yielded comparable ATP hydrolytic rates while the kinase inactive mutant D1994A did not produce observable ATP hydrolysis. (B) All of the active LRRK2 variants, including G2019S, showed a decrease in ATPase activity when Mg^{2+} was replaced with Mn^{2+}. Titrations of either (C) Mg^{2+} or (D) Mn^{2+} in the presence or the absence of 50 μM LRRKtide were compared in a luciferase-based ATP detection assay. While the catalytic turnover of the ATP in the presence of LRRKtide reached a plateau at 5 mM Mg^{2+}, decreasing amount of Mn^{2+} from 10 to 1 mM activated LRRKtide-dependent ATP turnover and inhibited ATP hydrolysis.

inactive mutant, D1994A, showed minimal ATPase activity under both conditions (Figure 4B). Mn^{2+}, however, did not produce the same effect between kinase and ATPase activities for the G2019S variant. In the absence of LRRKtide, G2019S displayed a similar behavior observed with WT and R1441C

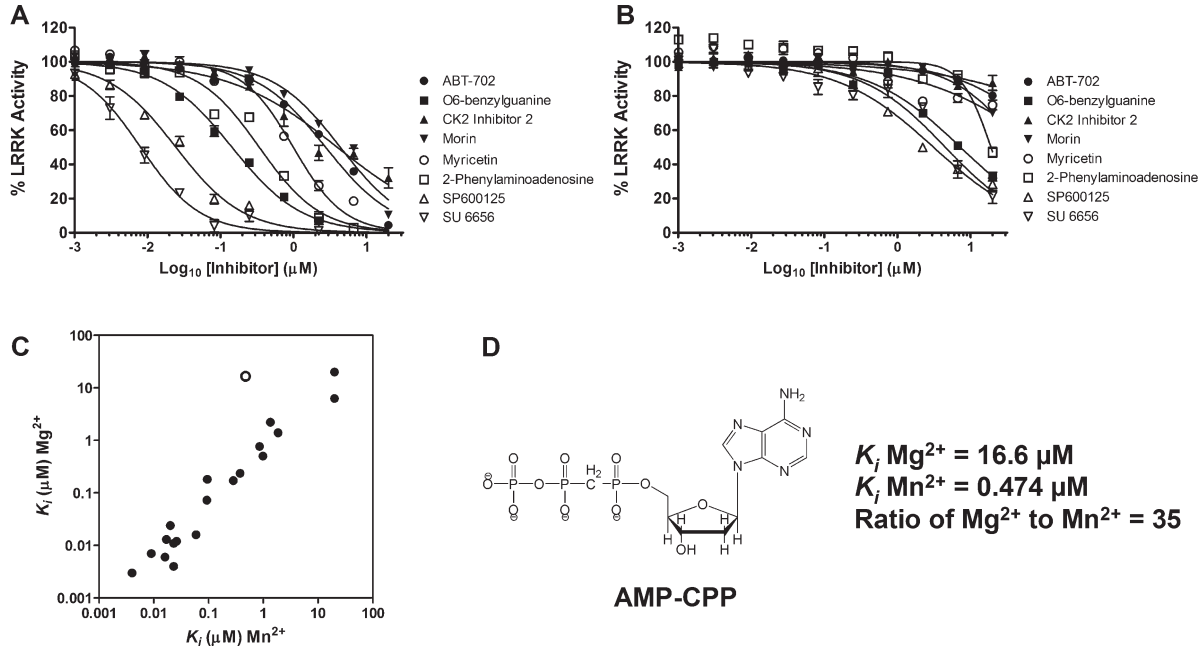

FIGURE 5: Representative titration curves of LRRK2 ATP-competitive inhibitors in either (A) 10 mM Mg^{2+} or (B) 1 mM Mn^{2+} reaction buffer in Transcreener ADP^2 assay. Compared to reactions performed with 100 μM ATP (at ATP K_m) in Mg^{2+} buffer, IC_{50} values were shifted higher in Mn^{2+} buffer where 100 μM ATP was ~55-fold higher than ATP K_m. (C) Correlation of inhibitor K_i values derived from IC_{50} obtained with 100 μM ATP for 10 mM Mg^{2+} and 10 μM ATP for 1 mM Mn^{2+} to allow full dose−response curves showed good correlation (< 5-fold difference) except one compound (open circle), the ATP analogue AMP-CPP. (D) AMP-CPP exhibited a shift in K_i values from 16.6 to 0.474 μM in Mg^{2+} and Mn^{2+}, respectively.

and had a decrease in ATP turnover when Mn^{2+} was substituted for Mg^{2+} in the reaction (Figure 4B). This decrease in ATP turnover is opposite to the increase in Mn^{2+}-mediated G2019S phosphorylation activity (Figure 1E). Titration of ATP against G2019S without the peptide substrate showed that the ATP K_m values were similar between ATPase and kinase activities and also displayed a comparable shift between the two buffers (ATP K_m Mg^{2+} = 88 ± 15 μM; ATP K_m Mn^{2+} = 1.5 ± 0.4 μM) but reduced the V_{max} in Mn^{2+}-mediated ATPase activity by about 8-fold (V_{max} Mg^{2+} = 0.211 ± 0.013 μmol/min; V_{max} Mn^{2+} = 0.026 ± 0.001 μmol/min). Again, this result is consistent with the hypotheses that (1) the catalytic turnover of ATP observed in the two enzymatic activities both came from LRRK2 protein and (2) the two activities were unlikely to be caused by the presence of two or more subpopulations of the LRRK2.

To confirm that Mn^{2+} differentially modulates G2019S kinase and ATPase activities, a reaction was set up using 10 μM ATP either with or without 50 μM LRRKtide in luciferase-based ATP detection assay. The chosen substrate concentrations produced a ratio of approximately 1:2 ATP turnover between ATPase activity alone (no LRRKtide) and ATPase/kinase activity combined (plus LRRKtide) at divalent ion concentrations ranging from 10 to 15 mM (Figure 4C,D). Titration of divalent ions showed that while the LRRKtide-dependent turnover of ATP increased with increasing levels of Mg^{2+} and reached a plateau at 5 mM Mg^{2+}, the catalytic turnover of ATP in the presence of the LRRKtide substrate was significantly enhanced with lower levels of Mn^{2+} (Figure 4C,D). These data are consistent with the differential V_{max} of G2019S kinase activity observed in the divalent ion titrations (Figure 3). The specific activities of G2019S in this experiment calculated based on the percent ATP conversion are ~200 h^{-1} and ≥450 h^{-1} for 5 mM Mg^{2+} and 1 mM Mn^{2+}, respectively. Under the same assay conditions (10 μM ATP and 50 μM LRRKtide in a luciferase-based ATP assay), the specific activity shown in the optimal 156 μM Mn^{2+}/5 mM Mg^{2+} mixture is ~325 h^{-1}, which is lower than the specific activity derived from Mn^{2+} alone. In the absence of LRRKtide, ATP hydrolysis by G2019S was not affected by various tested concentrations of Mg^{2+} that also showed no effect on the kinase activity, but the ATP hydrolysis was decreased by the low levels of Mn^{2+} which was the same range of Mn^{2+} capable of activating G2019S kinase activity. If LRRK2's ATPase and kinase activities are additive, our data suggest that low concentrations of Mn^{2+} could shift G2019S from having significant ATPase activity (~50%) to having predominantly kinase activity (>90%). Therefore, this modulation of the overall activity is due to a combination of ATPase inhibition and kinase activation for the G2019S variant. To understand the molecular mechanism behind the differential effects of Mn^{2+} on G2019S ATPase and kinase activities will require structural characterization of the metal-bound kinase active site.

ATP Analogue Inhibitors Show Higher Potency in the Presence of Mn^{2+}. Previously, a set of ATP-competitive inhibitors were shown to yield weaker IC_{50} values against LRRK2 I2020T when compared to LRRK2 WT and G2019S due to I2020T's lower ATP K_m value (*26*). With the approximately 100-fold shift in the ATP K_m between the two divalent ion mediated reactions, ATP-competitive inhibitors were also expected to produce significantly different IC_{50} values at a given concentration of ATP. A set of Sigma LOPAC compounds were tested in Transcreener ADP^2 assay against LRRK2 at 100 μM ATP under both Mn^{2+} and Mg^{2+} conditions (Figure 5A,B). All of the compounds showed a significant loss in inhibitory potency in the presence of Mn^{2+} ([ATP] at 55-fold over K_m) compared to Mg^{2+} ([ATP] at K_m). However, when K_i values obtained from applying the Cheng−Prusoff equation (*22*) were compared between the reactions mediated by the two different divalent ions, all compounds except one yielded good correlation with ≤5-fold

Table 1: IC_{50} Values of ATP Competitive Inhibitors and ATP Analogues in Competitive Binding FP Assay

LRRK2		IC_{50} (μM) Mg^{2+}	IC_{50} (μM) Mn^{2+}	ratio
G2019S	inhibitor A	0.322	0.143	2
	inhibitor B	0.153	0.094	2
	inhibitor C	0.116	0.056	2
	staurosporine	0.004	0.004	1
	AMP-CPP	334	0.127	2630
	ATP	395	1.46	271
	ATPγS	408	6.61	62
	ADP	629	26.0	24
WT	AMP-CPP	795	2.57	309
	ATP	718	4.05	177
	ATPγS	725	24.8	29
	ADP	1259	73.3	17

differences between the two values (Figure 5C). Not surprisingly, the compound that displayed a 35-fold more potent K_i in Mn^{2+} is an ATP analogue, AMP-CPP (Figure 5D). Whether a small molecule inhibitor that is not an ATP-like molecule will show selectivity for LRRK2 enzyme in the presence of different divalent ions will require testing with a larger array of small molecule inhibitors.

Divalent Manganese Enhances the Relative Affinity of both ATP and ADP to the LRRK2 Kinase Active Site. The data from steady-state kinetic characterization showed a significant change in ATP K_m with a change in the divalent metal ions. Using an AlexaFluor 647-labeled kinase active site binder (kinase tracer 236) as a probe whose binding affinity was not affected by divalent ions (data not shown), the competitive FP binding assay showed that Mn^{2+} increased the apparent ATP, ATPγS, and AMP-CPP binding affinity (IC_{50}) to G2019S by greater than 50-fold compared to Mg^{2+} (Table 1). Binding was increased to a lesser extent in WT enzyme. These data confirmed that the change in ATP K_m in the Mn^{2+} buffer was due in large part to a change in the ATP binding affinity. Other ATP-competitive small molecule inhibitors, compounds A−C and staurosporine, showed roughly equivalent affinity to the enzyme between Mn^{2+} and Mg^{2+} buffers. This result is consistent with the enzyme inhibition dose−response study where non-ATP-like small molecules had comparable K_i values between Mn^{2+} and Mg^{2+}. These data also suggest that, between the two divalent ions, any potential difference in the LRRK2 active site recognition by small molecules may require the compound binding to amino acid residues important to metal ion binding. Furthermore, among the nucleotide analogues containing triphosphates (AMP-CPP, ATP, and ATPγS), the apparent binding affinity (IC_{50}) to each LRRK2 variant in the presence of Mg^{2+} shown in this competition binding assay was constant (IC_{50} = 334, 395, and 408 μM, respectively, for G2019S and IC_{50} = 795, 718, and 725 μM, respectively, for WT). The three nucleotides, however, showed differential binding affinity in the presence of Mn^{2+} (IC_{50} = 0.127, 1.46, and 6.61 μM, respectively, for G2019S and IC_{50} = 2.57, 4.05, and 24.8 μM, respectively, for WT) with the binding affinity following the order of AMP-CPP > ATP > ATPγS for both G2019S and WT. This result is consistent with the hypothesis that the two divalent ions may have different coordination with ATP in the LRRK2 active site either during the ATP−metal complex formation or during the phosphotransfer transition steps. Moreover, the affinity difference between ADP and the three ATP analogues was much larger in Mn^{2+} buffer than in Mg^{2+} buffer (< 2-fold for Mg^{2+} and 3−18-fold for Mn^{2+}), suggesting that the interaction between the γ-phosphate and Mn^{2+} contributed significantly to the metal−nucleotide binding. Interestingly, similar to ATP, ADP also displayed a higher affinity to the enzyme in the presence of Mn^{2+}. It has been suggested that a change in the rate-limiting ADP release step can modulate the k_{cat} as seen with cAMP-dependent protein kinase (PKA) (*29*, *30*); therefore, an increase in the ADP affinity by Mn^{2+} could potentially contribute to the observed decrease in the LRRK2 catalytic rate. Finally, the competitive FP assay data also suggest that the binding of ATP to the active site does not require prior peptide substrate binding, a finding that is consistent with the enzyme's intrinsic ATPase activity.

DISCUSSION

In this study we have demonstrated that, under certain reaction conditions, the phosphorylation of MBP and LRRKtide by the G2019S mutant of LRRK2 can be selectively activated by Mn^{2+}. This increase in substrate phosphorylation by G2019S appears to be due to a combination of ATPase inhibition and kinase activation. Compared to Mg^{2+}, Mn^{2+} provided a favorable k_{cat}/K_m for all of the active LRRK2 variants tested, and this enhancement in catalytic efficiency was due to a 100-fold decrease in ATP K_m values. Mn^{2+}, however, also significantly reduced k_{cat} on all variants except G2019S. As a result, the apparent difference in the kinase activity between G2019S and other LRRK2 variants was enhanced in the presence of Mn^{2+} at ATP concentrations in excess to their K_m (e.g., $\geq$10 μM). This distinct behavior of G2019S suggests that the G2019 residue at the metal binding domain plays a critical role in modulating ATP catalytic turnover rather than ATP binding affinity, and the mutation to a serine residue may provide a favorable transition state for the phosphotransfer step especially for the Mn^{2+}-mediated reaction. In addition, our current data also showed that while increasing the concentration of Mg^{2+} above 1 mM increased V_{max} for G2019S without affecting ATP K_m, the V_{max} values obtained with Mn^{2+} were enhanced with Mn^{2+} concentrations well below the millimolar range. These ranges of optimal activities observed for each of the divalent ions are similar to those observed for cAMP-dependent kinase. The K_{app} values for enhancing the binding of labeled adenosine nucleotide to the kinase catalytic domain of cAMP-dependent kinase for Mn^{2+} and Mg^{2+} were shown to be 31 μM and 2.82 mM, respectively (*31*). For CSK and Src kinases, the increasing V_{max} for the Mg^{2+}-mediated reaction beyond the saturation concentration of Mg^{2+}−ATP complex formation has been thought to be attributed to a second metal binding (*27*) potentially also in the kinase active site, and G2019S activation by increasing concentration of Mg^{2+} may be parallel to this scenario. Taken together, the differential effects of divalent ions on ATP K_m and V_{max} values suggest potential differences in metal−ATP coordination in LRRK2 active sites. Although there are various possible structures of metal−ATP complexes, it is known that metal binding to the γ-phosphate group is essential for catalyzing nucleophilic attack by water molecule or amino acid side chain of the protein substrate. Because of the differences in the ionic radii and the strength of Lewis acidity among different divalent ions (*32*), the structure of the metal−ATP−LRRK2 complex may be different between Mg^{2+} and Mn^{2+}. Mn^{2+}, as a slightly larger ion and a softer Lewis acid, has a preference for coordinating in an environment mixed with some

weaker Lewis bases such as nitrogen and sulfur, whereas Mg^{2+} binds almost exclusively with oxyanions (*32*, *33*). Mg^{2+} and Mn^{2+}, for example, have been shown in a crystallographic structure to bind at two distinct locations in the phosphoenolpyruvate carboxykinase (PEPCK) active site, with Mg^{2+} chelating both the β- and γ-phosphate of ATP while Mn^{2+} binds to only the γ-phosphate. The two divalent ions coexist in the PEPCK active site making contacts with different amino acid residues (*33*). Structural insights into the LRRK2 active site will be the key in elucidating potential causes for the variations observed in ATP binding and catalysis among different divalent ions for each LRRK2 variant.

Using an active site binding probe, the competitive FP binding assay confirmed that Mn^{2+} caused a significant enhancement in nucleotide binding in the LRRK2 active site compared to Mg^{2+} supporting the hypothesis that the change in the apparent nucleotide affinity contributed to the decrease in the observed ATP K_m. The binding of the ATP nucleotide in the absence of peptide/protein substrate is also consistent with the observed LRRK2 ATPase activity. Furthermore, while no difference in the apparent binding was observed among the various ATP analogues in the presence of Mg^{2+}, the LRRK2 active site affinities among the nucleotide analogues were different in the presence of Mn^{2+}, with AMP-CPP showing 52- and 10-fold higher affinity than ATPγS for G2019S and WT, respectively. This difference in affinity suggests that the active site of Mn^{2+}-bound LRRK2 is sensitive to the slight conformational changes in the nucleotide induced by the changes in the phosphodiester bonds and the substitutions on the phosphate group(s). This different sensitivity toward the phosphodiester backbone of ATP between Mg^{2+} and Mn^{2+} is consistent with the hypothesis that the two divalent ions might coordinate differently with ATP at the LRRK2 active site. If the two divalent metal ions do bind to both ATP and the LRRK2 active site differently, Mg^{2+} and Mn^{2+} could potentially induce subtly different conformations in the kinase active site. If conformation of the ATP binding pocket can indeed be modulated by the divalent ions, the active site recognition by small molecule ATP-competitive inhibitors could be affected as well. With the limited compounds tested in this study, however, no inhibitor except AMP-CPP yielded a different K_i between Mn^{2+}- and Mg^{2+}-mediated kinase reactions, suggesting that any effect on small molecule recognition may require direct interaction of the molecule with the divalent ions and/or with the amino acid residues involved in coordinating the ATP phosphotransfer transition state. This hypothesis, however, needs to be investigated with a more diverse array of small molecule inhibitors.

Previously, Reichling and Riddle have shown that inhibitors yield different inhibitory potencies between I2020T and G2019S due to their difference in ATP K_m values (*26*). Even though the apparent K_i values of the non-ATP analogue inhibitors tested in this study were comparable between Mg^{2+} and Mn^{2+}, the effective inhibitory potency at cellular ATP concentrations can be very different depending on which physiologically relevant divalent ion LRRK2 utilizes in cells. With physiologically relevant ATP concentrations at the millimolar range in cells, the cellular IC_{50} of an ATP-competitive inhibitor can be shifted to a weaker value from its K_i by 1000-fold with Mn^{2+}-LRRK2 but only by 10-fold with Mg^{2+}-LRRK2. The common assumption that Mg^{2+} is the physiologically relevant metal ion for kinases because of its abundance in cells (single digit millimolar) suggests that LRRK2 would likely utilize Mg^{2+} for enzymatic catalysis. With WT and R1441C variants, the large inhibitory effects of Mn^{2+} shown *in vitro* on their k_{cat} could suggest that utilizing Mn^{2+} instead of Mg^{2+} at millimolar ATP levels (excess to its K_m) is catalytically inefficient. This could support the hypothesis that Mg^{2+} is likely the preferred catalytic cofactor for productive activity. With G2019S, however, the negative impact of Mn^{2+} on the k_{cat} is minimal, and the concentration of Mn^{2+} required for optimal G2019S kinase activity is in the approximate range of its physiological concentration (micromolar) which is significantly lower than the optimal concentration required for Mg^{2+}. With ATP K_m at single digit micromolar for G2019S, a kinase reaction mediated by the physiological level of Mn^{2+} is certainly feasible. The titration data of Mn^{2+} into Mg^{2+} suggest that, at vast molar excess of 5 mM Mg^{2+}, Mn^{2+} at micromolar levels is still capable of activating G2019S kinase activity, further lending support to our hypothesis that a kinase reaction mediated by the physiological level of Mn^{2+} is feasible. However, an obvious caveat to this hypothesis is the disparity that may exist between *in vivo* conditions and *in vitro* assays used in our studies. Whether the G2019S mutation at the metal binding domain may truly influence the utilization of different divalent ions for its catalytic activity *in vivo* compared to other variants will require further investigation using endogenous proteins in a cellular environment.

ACKNOWLEDGMENT

We thank Dr. Cristina Lewis, Dr. Maureen Beresini, Dr. Ryan Watts, Dr. Adam Johnson, Dr. Zachary Sweeney, and Amy Gustafson for critically reviewing the manuscript and Dr. John Moffat and Dr. Jiansheng Wu for many helpful discussions.

REFERENCES

1. Zimprich, A., Biskup, S., Leitner, P., Lichtner, P., Farrer, M., Lincoln, S., Kachergus, J., Hulihan, M., Uitti, R. J., Calne, D. B., Stoessl, A. J., Pfeiffer, R. F., Patenge, N., Carbajal, I. C., Vieregge, P., Asmus, F., Muller-Myhsok, B., Dickson, D. W., Meitinger, T., Strom, T. M., Wszolek, Z. K., and Gasser, T. (2004) Mutations in LRRK2 cause autosomal-dominant parkinsonism with pleomorphic pathology. *Neuron 44*, 601–607.
2. Ko, H. S., Bailey, R., Smith, W. W., Liu, Z., Shin, J. H., Lee, Y. I., Zhang, Y. J., Jiang, H., Ross, C. A., Moore, D. J., Patterson, C., Petrucelli, L., Dawson, T. M., and Dawson, V. L. (2009) CHIP regulates leucine-rich repeat kinase-2 ubiquitination, degradation, and toxicity. *Proc. Natl. Acad. Sci. U.S.A. 106*, 2897–2902.
3. Hurtado-Lorenzo, A., and Anand, V. S. (2008) Heat shock protein 90 modulates LRRK2 stability: potential implications for Parkinson's disease treatment. *J. Neurosci. 28*, 6757–6759.
4. Wang, L., Xie, C., Greggio, E., Parisiadou, L., Shim, H., Sun, L., Chandran, J., Lin, X., Lai, C., Yang, W. J., Moore, D. J., Dawson, T. M., Dawson, V. L., Chiosis, G., Cookson, M. R., and Cai, H. (2008) The chaperone activity of heat shock protein 90 is critical for maintaining the stability of leucine-rich repeat kinase 2. *J. Neurosci. 28*, 3384–3391.
5. Gandhi, P. N., Wang, X., Zhu, X., Chen, S. G., and Wilson-Delfosse, A. L. (2008) The Roc domain of leucine-rich repeat kinase 2 is sufficient for interaction with microtubules. *J. Neurosci. Res. 86*, 1711–1720.
6. Smith, W. W., Pei, Z., Jiang, H., Dawson, V. L., Dawson, T. M., and Ross, C. A. (2006) Kinase activity of mutant LRRK2 mediates neuronal toxicity. *Nat. Neurosci. 9*, 1231–1233.
7. West, A. B., Moore, D. J., Biskup, S., Bugayenko, A., Smith, W. W., Ross, C. A., Dawson, V. L., and Dawson, T. M. (2005) Parkinson's disease-associated mutations in leucine-rich repeat kinase 2 augment kinase activity. *Proc. Natl. Acad. Sci. U.S.A. 102*, 16842–16847.
8. Jaleel, M., Nichols, R. J., Deak, M., Campbell, D. G., Gillardon, F., Knebel, A., and Alessi, D. R. (2007) LRRK2 phosphorylates moesin at threonine-558: characterization of how Parkinson's disease mutants affect kinase activity. *Biochem. J. 405*, 307–317.
9. Paisan-Ruiz, C., Jain, S., Evans, E. W., Gilks, W. P., Simon, J., van der Brug, M., Lopez de Munain, A., Aparicio, S., Gil, A. M.,

Khan, N., Johnson, J., Martinez, J. R., Nicholl, D., Carrera, I. M., Pena, A. S., de Silva, R., Lees, A., Marti-Masso, J. F., Perez-Tur, J., Wood, N. W., and Singleton, A. B. (2004) Cloning of the gene containing mutations that cause PARK8-linked Parkinson's disease. *Neuron 44*, 595–600.

10. Anand, V. S., Reichling, L. J., Lipinski, K., Stochaj, W., Duan, W., Kelleher, K., Pungaliya, P., Brown, E. L., Reinhart, P. H., Somberg, R., Hirst, W. D., Riddle, S. M., and Braithwaite, S. P. (2009) Investigation of leucine-rich repeat kinase 2: enzymological properties and novel assays. *FEBS J. 276*, 466–478.
11. Greggio, E., Jain, S., Kingsbury, A., Bandopadhyay, R., Lewis, P., Kaganovich, A., van der Brug, M. P., Beilina, A., Blackinton, J., Thomas, K. J., Ahmad, R., Miller, D. W., Kesavapany, S., Singleton, A., Lees, A., Harvey, R. J., Harvey, K., and Cookson, M. R. (2006) Kinase activity is required for the toxic effects of mutant LRRK2/dardarin. *Neurobiol. Dis. 23*, 329–341.
12. Ito, G., Okai, T., Fujino, G., Takeda, K., Ichijo, H., Katada, T., and Iwatsubo, T. (2007) GTP binding is essential to the protein kinase activity of LRRK2, a causative gene product for familial Parkinson's disease. *Biochemistry 46*, 1380–1388.
13. Luzon-Toro, B., Rubio de la Torre, E., Delgado, A., Perez-Tur, J., and Hilfiker, S. (2007) Mechanistic insight into the dominant mode of the Parkinson's disease-associated G2019S LRRK2 mutation. *Hum. Mol. Genet. 16*, 2031–2039.
14. Weiss, B. (2008) ROCO kinase activity is controlled by internal GTPase function. *Sci. Signaling 1*, pe27.
15. West, A. B., Moore, D. J., Choi, C., Andrabi, S. A., Li, X., Dikeman, D., Biskup, S., Zhang, Z., Lim, K. L., Dawson, V. L., and Dawson, T. M. (2007) Parkinson's disease-associated mutations in LRRK2 link enhanced GTP-binding and kinase activities to neuronal toxicity. *Hum. Mol. Genet. 16*, 223–232.
16. Lewis, P. A., Greggio, E., Beilina, A., Jain, S., Baker, A., and Cookson, M. R. (2007) The R1441C mutation of LRRK2 disrupts GTP hydrolysis. *Biochem. Biophys. Res. Commun. 357*, 668–671.
17. Romani, A., and Scarpa, A. (1992) Regulation of cell magnesium. *Arch. Biochem. Biophys. 298*, 1–12.
18. Adams, J. A. (2001) Kinetic and catalytic mechanisms of protein kinases. *Chem. Rev. 101*, 2271–2290.
19. Greggio, E., and Cookson, M. R. (2009) Leucine-rich repeat kinase 2 mutations and Parkinson's disease: three questions. *ASN Neuro. 1*, 13–24.
20. Nolen, B., Taylor, S., and Ghosh, G. (2004) Regulation of protein kinases; controlling activity through activation segment conformation. *Mol. Cell 15*, 661–675.
21. Johnson, L. N., Noble, M. E., and Owen, D. J. (1996) Active and inactive protein kinases: structural basis for regulation. *Cell 85*, 149–158.
22. Cheng, Y., and Prusoff, W. H. (1973) Relationship between the inhibition constant (K1) and the concentration of inhibitor which causes 50% inhibition (I50) of an enzymatic reaction. *Biochem. Pharmacol. 22*, 3099–3108.
23. Tuazon, P. T., Chinwah, M., and Traugh, J. A. (1998) Autophosphorylation and protein kinase activity of p21-activated protein kinase gamma-PAK are differentially affected by magnesium and manganese. *Biochemistry 37*, 17024–17029.
24. Yuan, C. J., Huang, C. Y., and Graves, D. J. (1993) Phosphorylase kinase, a metal ion-dependent dual specificity kinase. *J. Biol. Chem. 268*, 17683–17686.
25. Grace, M. R., Walsh, C. T., and Cole, P. A. (1997) Divalent ion effects and insights into the catalytic mechanism of protein tyrosine kinase Csk. *Biochemistry 36*, 1874–1881.
26. Reichling, L. J., and Riddle, S. M. (2009) Leucine-rich repeat kinase 2 mutants I2020T and G2019S exhibit altered kinase inhibitor sensitivity. *Biochem. Biophys. Res. Commun. 384*, 255–258.
27. Sun, G., and Budde, R. J. (1997) Requirement for an additional divalent metal cation to activate protein tyrosine kinases. *Biochemistry 36*, 2139–2146.
28. Montes, S., Alcaraz-Zubeldia, M., Muriel, P., and Rios, C. (2001) Striatal manganese accumulation induces changes in dopamine metabolism in the cirrhotic rat. *Brain Res. 891*, 123–129.
29. Adams, J. A., and Taylor, S. S. (1993) Divalent metal ions influence catalysis and active-site accessibility in the cAMP-dependent protein kinase. *Protein Sci. 2*, 2177–2186.
30. Cook, P. F. (1982) Kinetic studies to determine the mechanism of regulation of bovine liver glutamate dehydrogenase by nucleotide effectors. *Biochemistry 21*, 113–116.
31. Bhatnagar, D., Roskoski, R., Jr., Rosendahl, M. S., and Leonard, N. J. (1983) Adenosine cyclic 3′,5′-monophosphate dependent protein kinase: a new fluorescence displacement titration technique for characterizing the nucleotide binding site on the catalytic subunit. *Biochemistry 22*, 6310–6317.
32. Tam, S.-C., and Williams, R. J. P. (1985) Electrostatics and biological systems, in Structure and Bonding, pp 103−151, Springer, Berlin/Heidelberg.
33. Tari, L. W., Matte, A., Goldie, H., and Delbaere, L. T. (1997) Mg^{2+}-Mn^{2+} clusters in enzyme-catalyzed phosphoryl-transfer reactions. *Nat. Struct. Biol. 4*, 990–994.